Characterizing the *FY-3A* Microwave Temperature Sounder Using the ECMWF Model

QIFENG LU

National Satellite Meteorological Center, China Meteorological Administration, Beijing, China

WILLIAM BELL, PETER BAUER, NIELS BORMANN, AND CAROLE PEUBEY

ECMWF, Shinfield Park, Reading, United Kingdom

(Manuscript received 4 October 2010, in final form 8 March 2011)

ABSTRACT

China's *Feng-Yun-3A* (*FY-3A*), launched in May 2008, is the first in a series of seven polar-orbiting meteorological satellites planned for the next decade by China. The *FY-3* series is set to become an important data source for numerical weather prediction (NWP), reanalysis, and climate science. *FY-3A* is equipped with a microwave temperature sounding instrument (MWTS). This study reports an assessment of the MWTS instrument using the ECMWF NWP model, radiative transfer modeling, and comparisons with equivalent observations from the Advanced Microwave Sounding Unit-A (AMSU-A). The study suggests the MWTS instrument is affected by biases related to large shifts, or errors, in the frequency of the channel passbands as well as radiometer nonlinearity. The passband shifts, relative to prelaunch measurements, are 55, 39, and 33 MHz for channels 2–4, respectively. Relative to the design specification the shifts are 60, 80, and 83 MHz, with uncertainties of ±2.5 MHz. The radiometer nonlinearity results in a positive bias in measured brightness temperatures and is manifested as a quadratic function of measured scene temperatures. By correcting for both of these effects the quality of the MWTS data is improved significantly, with the standard deviations of the (observed minus simulated) differences based on short-range forecast fields reduced by 30%–50% relative to simulations using prelaunch measurements of the passband, to values close to those observed for AMSU-A-equivalent channels. The new methodology could be applied to other microwave temperature sounding instruments and illustrates the value of NWP fields for the on-orbit characterization of satellite sensors.

1. Introduction

China's *Feng-Yun-3A* (*FY-3A*), launched in May 2008, is the first in a series of seven meteorological satellites due to be launched in the period leading up to 2020 by China's Meteorological Administration. The *FY-3A* payload includes four instruments of particular interest to numerical weather prediction (NWP) and climate science: microwave temperature and humidity sounders, a microwave imager, and an infrared sounder. This study is concerned with the on-orbit performance of the *FY-3A* microwave temperature sounder (MWTS), the characteristics of which are summarized in Table 1. The MWTS is a cross-track scanning radiometer with a swath width of 2250 km, a nadir footprint size of 62 km, and 15 fields of view per scan line. *FY-3B*, due for launch in 2010 at the time of this writing, will also carry an MWTS instrument. MWTS features four channels, which are illustrated in Fig. 1. The weighting functions for the sounding channels (2–4) are shown in Fig. 2, together with typical mean temperature profiles for different latitude bands. The remaining five platforms (*FY-3C*–*FY-3G*) will carry a more advanced microwave sounder with 13 channels, similar in specification to the Advanced Microwave Sounding Unit-A (AMSU-A; see Goodrum et al. 2000), which is carried on the *National Oceanic and Atmospheric Administration* (*NOAA*)*-15* to *NOAA-19* platforms, as well as National Aeronautics and Space Administration's (NASA's) *Aqua* platform and the European Organisation for the Exploitation of Meteorological Satellites's (EUMETSAT's) *Meteorological Operation* (*MetOp*)*-A* satellite. MWTS is similar, but not identical, in specification to the Microwave Sounding Units (MSUs)

Corresponding author address: Qifeng Lu, National Satellite Meteorological Center, China Meteorological Administration, 100081 Beijing, China.
E-mail: qifeng.lu@ecmwf.int

DOI: 10.1175/JTECH-D-10-05008.1

TABLE 1. *FY-3A* MWTS channel characteristics.

Channel No. (equivalent AMSU-A)	Frequency (GHz; design)	Bandwidth (MHz)	NEΔT (prelaunch; K)
1 (3)	50.3	180	0.5
2 (5)	53.596 ± 0.115	2 × 170	0.4
3 (7)	54.94	400	0.4
4 (9)	57.29	330	0.4

that were carried on board the NOAA Television and Infrared Observation Satellite (TIROS)-N and Polar-Orbiting Environmental Satellite (POES) series TIROS-N–*NOAA-14*. Although initial prototype designs for the MWTS had passbands equivalent to those of the MSU, the channel passbands of the *FY-3A* flight model (Dong et al. 2009) are identical to the equivalent AMSU-A channels to give continuity with existing NOAA operational instruments. As a preparatory mission it is important that any instrument-related biases in the data are characterized, so that that these biases can be corrected for the *FY-3A* MWTS and subsequent sensors, and can be dealt with appropriately in NWP data assimilation systems. This study presents evidence of two distinct biases in the MWTS measurements based on comparisons with ECMWF model fields and with equivalent AMSU-A observations.

Until the recent advent of advanced IR sounding instruments, microwave temperature sounding data from high-performance radiometers was the single most important satellite data type in NWP data assimilation systems (English et al. 2004). Microwave temperature sounding data, by providing accurate information for the analysis of mass fields, is still a key component of NWP data assimilation systems. Recently developed advanced diagnostic tools have confirmed the continuing importance of microwave sounding data in NWP data assimilation systems (Cardinali 2009).

In today's variational assimilation systems, radiance measurements are routinely compared with NWP model fields mapped to brightness temperatures using radiative transfer modeling. Generally, differences will be nonzero and will comprise large-scale, slowly varying *systematic* biases, including radiative transfer modeling errors, as well as small-scale *day-to-day* features resulting from local errors in the forecast model fields, in addition to a purely *random* component from the instrument noise. In NWP assimilation systems it is crucial that the stationary, or quasi stationary, components of such biases (which may result from forecast model error, radiative transfer model error, or measurement error) are eliminated prior to assimilation, leaving only the errors in the model fields to be corrected. At ECMWF this is achieved using a variational bias correction scheme (Auligné et al. 2007; Dee 2005) in which the biases are represented by a relatively simple linear predictor model involving predictors derived from the model state variables and variables related to the observation geometry. The coefficients of this model form part of the analysis control vector and are estimated in each analysis cycle. It is important that this predictor model is able to represent the form of the biases observed. If this is not the case, for example, resulting from biases caused by a process that is not accurately represented by the

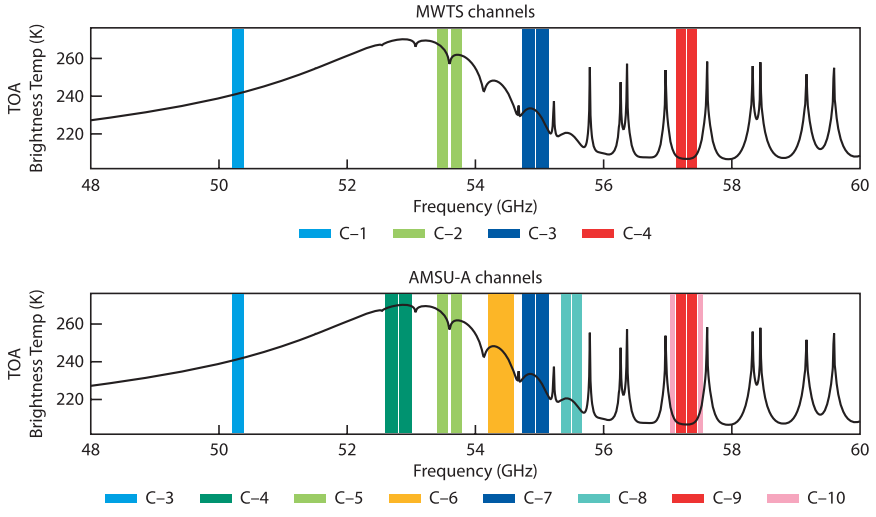

FIG. 1. Passbands for the four channels of the (top) *FY-3A* microwave temperature sounder and (bottom) AMSU-A channels 3–10. Also shown is a simulation of top-of-atmosphere brightness temperatures (K) for a typical tropical atmospheric profile.

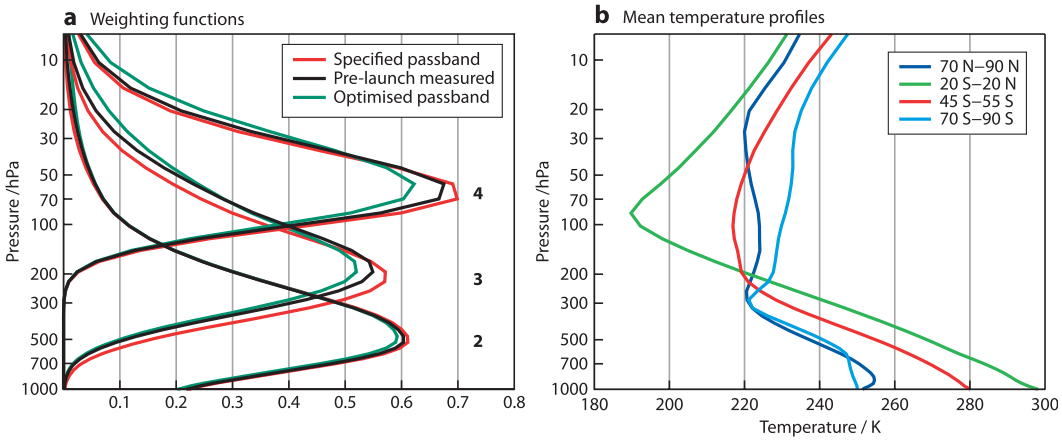

FIG. 2. (a) Weighting functions for MWTS channels 2, 3, and 4, based on design specification, prelaunch measurements, and optimized estimates of the passband center frequencies. (b) The mean temperature profiles for the latitude bands indicated (for 17 Sep 2008), from which the latitudinal dependence of the brightness temperature errors resulting from a (passband shift induced) vertical shift in the weighting function may be inferred.

linear predictor model, residual biases may remain in the data, which would degrade the accuracy of the analysis.

This is the case in this study where we present evidence that the *FY-3A* MWTS observations are affected by a shift in the passband center frequencies (relative to prelaunch measurements) for three of the four MWTS channels, as well as significant radiometer nonlinearity. This evidence is based on a comparison of observations with radiances modeled from ECMWF short-range forecast fields. The working assumption here is that the ECMWF model fields are sufficiently accurate to detect, partition, and quantify these instrument errors.

NWP models have been used in several investigations recently to characterize errors in microwave satellite observations. Bell et al. (2008) used NWP fields to detect and correct for several biases in the Special Sensor Microwave Imager/Sounder (SSMIS) observations, including biases related to reflector emission and warm load calibration anomalies. This study showed that for temperature sounding channels, instrument errors of several tenths of a kelvin could be detected using NWP model fields. Geer et al. (2010) showed that a bias related to reflector emission could be identified in observations from the Tropical Rainfall Measuring Mission (TRMM) Microwave Imager (TMI). The fidelity of the NWP short-range forecast field results from the large volume of satellite data, which determines the analysis used to produce the short-range forecasts. Of particular importance, with respect to the accuracy of the temperature fields in the midtroposphere to lower stratosphere where the MWTS channels have maximum sensitivity, are the observations from the advanced IR sounders [Atmospheric Infrared Sounder (AIRS) and Infrared Atmospheric Sounding Interferometer (IASI), see Collard and McNally (2009)]; six AMSU-A sensors carried onboard NOAA, NASA, and *MetOp-A* platforms; and data from a constellation of six GPS radio occultation (GPSRO) instruments (Healy and Thépaut 2006). Typical bias corrections for the advanced IR sounders for the temperature sounding channels are several tenths of a kelvin. For the AMSU-A instruments the bias corrections are generally below 1 K. The GPSRO observations, assimilated as bending angles, have very small absolute uncertainties and are assimilated without bias correction, thereby anchoring the NWP system.

Microwave sounding data, from MSU and AMSU, has been used extensively for climate studies aimed at estimating temperature trends in the troposphere and lower stratosphere (see Karl et al. 2006, and references therein). As part of the effort to reconcile differences between trends derived by independent researchers much effort has been focused on characterizing the nonlinear response of microwave radiometers to measured radiances accurately. Approaches based on a careful analysis of prelaunch data (Mo et al. 2001; Grody et al. 2004) as well as approaches that use satellite collocations in the polar regions have been reported (Zou et al. 2006). The approach presented here complements these established techniques in identifying, and correcting, two important instrument biases.

Regarding the problems associated with shifts in the center frequencies of passbands, a recent study (Peubey et al. 2011) has concluded that measurable degradations in NWP forecast quality can result from uncorrected passband shifts larger than 1.5 MHz.

In this study we report a new approach to diagnosing, and correcting, passband shifts and radiometer nonlinearity using NWP model fields. This approach has

been developed specifically for *FY-3A* MWTS, but is of general applicability to other microwave temperature sounders. In section 2 we describe the initial detection of the problem, through a comparison of the MWTS observations with AMSU-A observations, and some initial simulations. A sensitivity study that examined other possible sources [model bias, radiative transfer (RT) model bias, and a range of instrument calibration errors] of the biases detected in the MWTS observations is described in section 3, which concludes that the most likely causes for the biases are nonlinearity and passband shift. In section 4 we describe the approach used to optimize our estimate of the new instrument parameters. Finally, in section 5, we demonstrate the improvement in data quality through an inspection and analysis of first-guess departure fields prior to variational bias correction.

2. Comparisons with AMSU-A and initial simulations

MWTS data were obtained directly from China's Meteorological Administration. Limited information is available on the details of the preprocessing software, but it is known that an antenna pattern correction is performed and calibration data are averaged over seven consecutive scan lines to reduce calibration errors. Neither nonlinearity corrections nor corrections for spacecraft contamination were made in the version of the data used here.

A comparison of MWTS-observed brightness temperatures with equivalent *MetOp-A* AMSU-A observations gives some indication of possible biases in the MWTS observations. Figure 3 shows the measured brightness temperatures for a 12-h period during 17 September 2008 for both MWTS and the equivalent *MetOp-A* AMSU-A observations. *MetOp-A* [with an equatorial crossing time of 0930 local time (LT)] is in a very similar orbit plane to that of *FY-3A* (with an ascending node equatorial crossing time of 1005 LT), and hence both MWTS and AMSU-A show very similar coverage. From an inspection of the histograms of brightness temperatures it is evident that MWTS brightness temperatures, at the peaks in the histograms, are shifted by ~1–2 K for channels 2 and 3, and by 2–3 K for channel 4, relative to the AMSU-A observations. The shift is most evident for channels 2–4 because the dynamic range in measured brightness temperatures is relatively small (at 40–60 K) compared with the larger dynamical range for channel 1 (~140 K, not shown here), which has a significant contribution to the measured radiance from clouds and the surface. From Fig. 1 it is seen that these offsets are consistent with positive shifts in band center frequencies: positive shifts in passband center frequency cause negative shifts in brightness temperature for channels 2 and 3, and a positive shift for channel 4. At this stage though, there are other conceivable causes of this bias, which could alias into an apparent passband shift error. For channel 4, the shift of +2 K is most evident for the primary peak in the histogram, associated with observations in the tropics (at ~209 K). There is less evidence of a shift in the secondary maximum (at ~224 K) associated with measurements in the northern polar latitudes and an area of the Southern Ocean to the south of Australia.

As an initial step in understanding these biases, simulations of the expected brightness temperature error resulting from passband shift were carried out. The simulations used a line-by-line (LBL) radiative transfer model, based on the Millimeter Wave Propagation Model (MPM92) of Liebe et al. (1993; see also Liebe 1989; Liebe et al. 1992), to simulate brightness temperatures for specified levels of passband shift. Initially, a climatological set of atmospheric profiles was used to assess the expected latitudinal dependence of the passband shift–induced errors. The consistency of these error estimates with those expected from passband shifts of around 80 MHz (relative to design specification) was sufficient to warrant further investigation of the passband shift hypothesis.

The mechanism that results in this form of error is clear from Fig. 1, which shows that passband shifts result in the radiometer sampling different parts of the O_2 spectrum associated with different optical depths. This causes a displacement of the weighting function of the channel (see Fig. 2), which in turn results in the radiometer sampling higher or lower parts of the atmosphere. Depending on the local lapse rate in the region of the weighting function peak the shift in the brightness temperature can be either positive or negative. For example, for positive shifts in passband frequency for channel 4, the resulting upward shift in the weighting function results in positive shifts in measured brightness temperatures in the tropics where the lapse rate is strongly positive (~3 K km^{-1}) at the weighting function peak, but there are relatively small shifts in the northern polar latitudes where the lapse rate is near zero. This type of error is therefore a function of local lapse rate and not measured brightness temperature, which is the case for radiometer nonlinearity error (see section 3d below).

To further investigate the possible passband shift additional line-by-line modeling was conducted to assess the sensitivity of the (observation–model) fit for various passband shifts. Model geophysical fields (temperature and water vapor) were mapped to brightness temperatures for an ensemble of 15 000 observations, assuming passband center frequency shifts in the range of ±150 MHz. Standard deviation and mean differences (observation

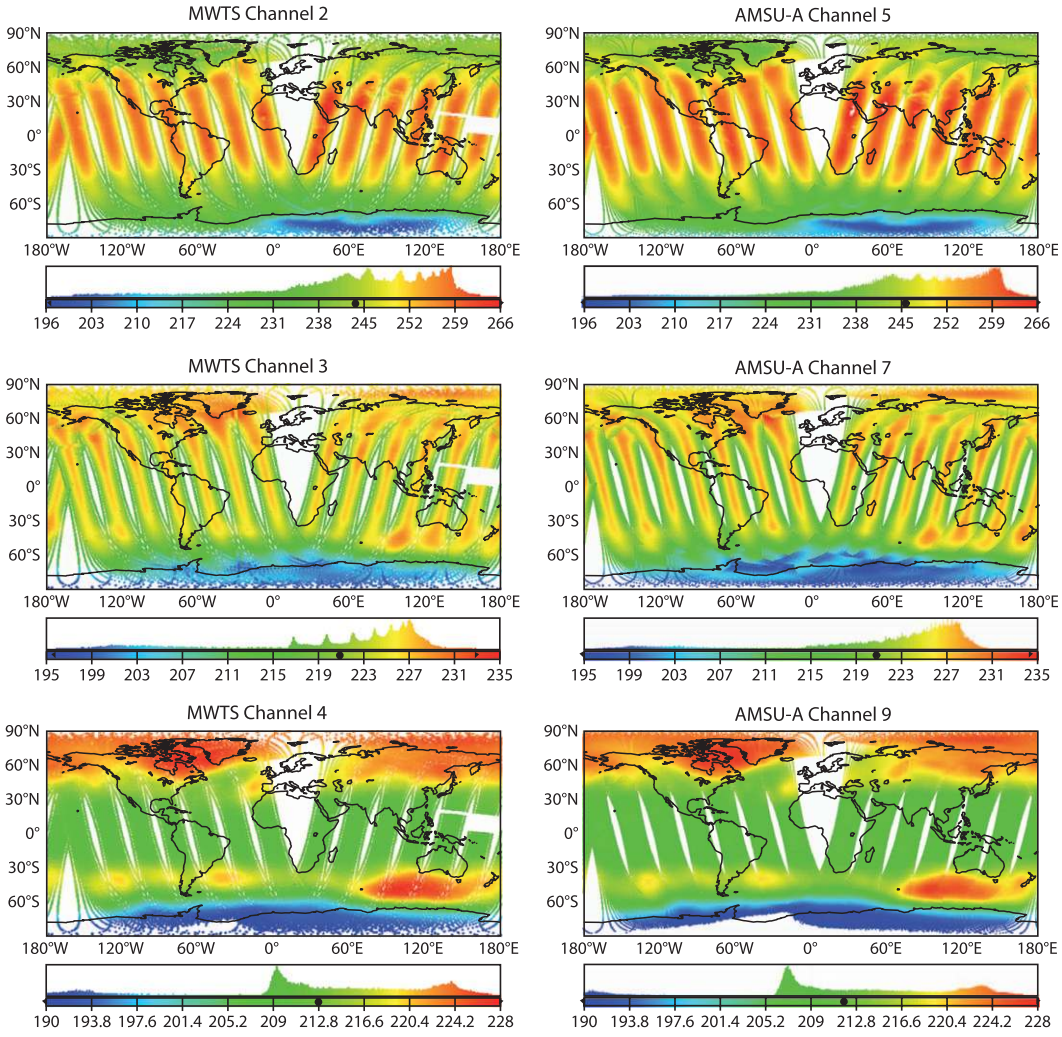

FIG. 3. Observed brightness temperatures for *FY3-A* MWTS and the equivalent *MetOp-A* AMSU-A channels. (left) The observed brightness temperatures for the *FY3-A* MWTS and (right) the brightness temperatures for the equivalent *MetOp-A* AMSU-A channels (for the 12-h cycle at 0000 UTC 17 Sep 2008) are shown. The spot at the base of the histograms indicates the mean brightness temperature for each plot.

minus simulation) were generated. The results are shown in Fig. 4. Two points are notable from this figure: first, the fit of model fields to the observed brightness temperatures is improved by assuming significant passband shifts for channels 2–4. These shifts halve the standard deviations of (observation − simulation) differences for channels 2–4 relative to those for the unshifted passbands, based on design-specified passbands. There are also significant improvements over simulations using passbands based on prelaunch measurements. Second, the position of the minimum in the standard deviation curves corresponds to a reduction in the magnitude of the mean difference between the observations and simulation; that is, both the magnitude and the structure of the (observation − simulation) differences are improved by assuming a passband shift of ~40–80 MHz. The biases remaining for channel 3 (+0.25 K) and channel 4 (+1 K) are still nonzero, and these are investigated further in section 3d below.

As a check of this approach, a similar analysis was carried out for *MetOp-A* AMSU-A channel 9, the results of which are shown in Fig. 4d. AMSU-A channel 9 does not show a double minimum structure, although a residual bias of 0.2 K remains in the simulations assuming the nominal designed passband specification.

3. Sensitivity study

Figure 4 gives a strong indication that the passband center frequency shift accounts for a significant fraction

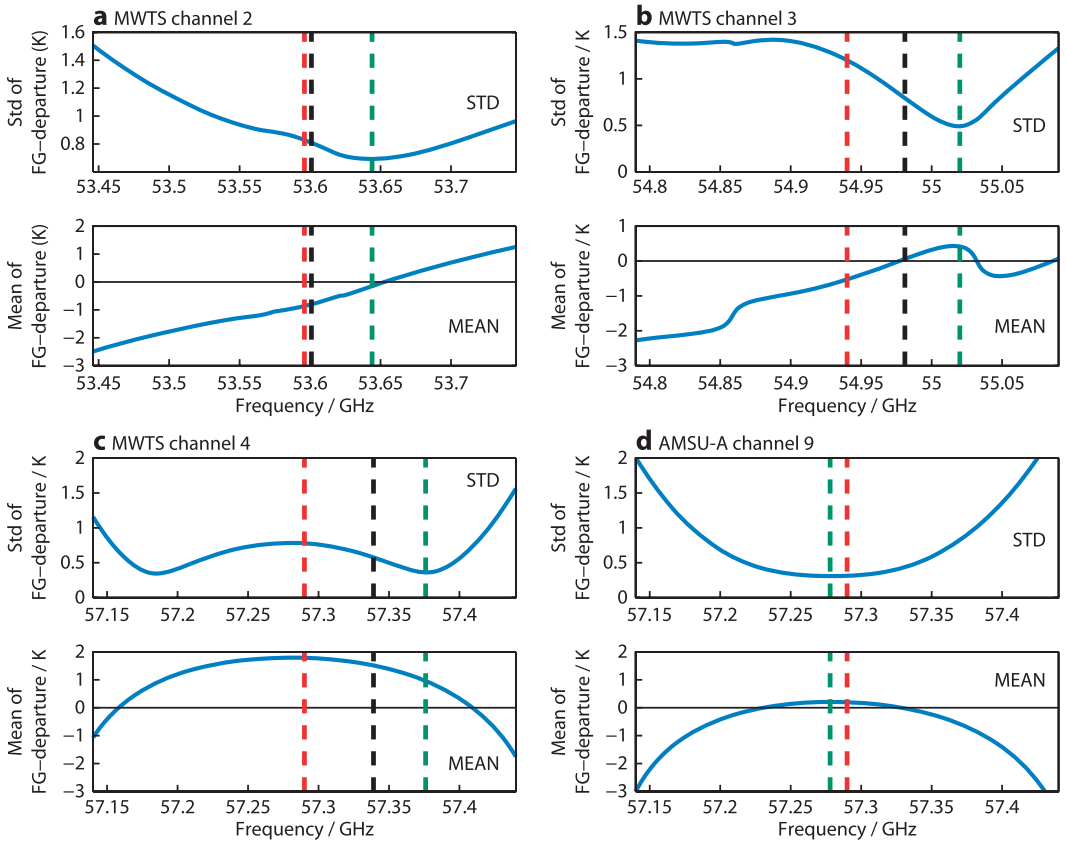

FIG. 4. The variation of (top) standard deviation and (bottom) mean of departures (observation minus model equivalent brightness temperatures) with passband shift for MWTS channels (a) 2, (b) 3, and (c) 4 and (d) AMSU-A channel 9. The design-specified passband center (dashed red line), passband based on prelaunch measurements (black dashed line), and frequency corresponding to the minimum in the first-guess departures (green dotted line) are shown.

of the variance in the uncorrected observation minus simulation differences (first-guess departures). To further test this hypothesis a sensitivity analysis was carried out to assess whether other errors—in the forecast model fields, in the radiative transfer model, or related to the instrument—could be manifested as apparent passband shift errors. Specifically, we assessed whether a range of errors would be manifested as a double minimum in the plots of the type shown in Fig. 4 for MWTS channel 4. The other possible sources of error are summarized schematically in Fig. 5. These errors can affect either the geophysical fields themselves, the mapping of these fields to brightness temperatures, or the observed values of brightness temperature. All of these errors can in principle contribute to the observed biases between observed and simulated brightness temperatures. The sensitivity analysis involved proposing hypothetical errors in model fields, the RT model, and the instrument, adding these to the (observation − simulated) fields for AMSU-A channel 9, and assessing the variation of the standard deviation of the differences as a function of assumed passband shift. Here the assumption is that the AMSU-A observations are free of significant errors related to the passband shift. The specific form and

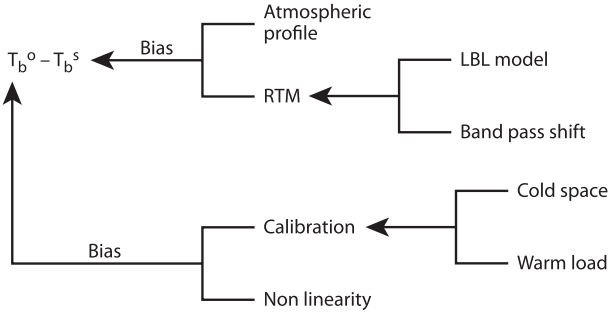

FIG. 5. The error terms considered in the sensitivity study, affecting the departures (observed minus simulated brightness temperatures), $T_b^o - T_b^s$ through the simulation (T_b^s), or directly affecting the observed values (T_b^o).

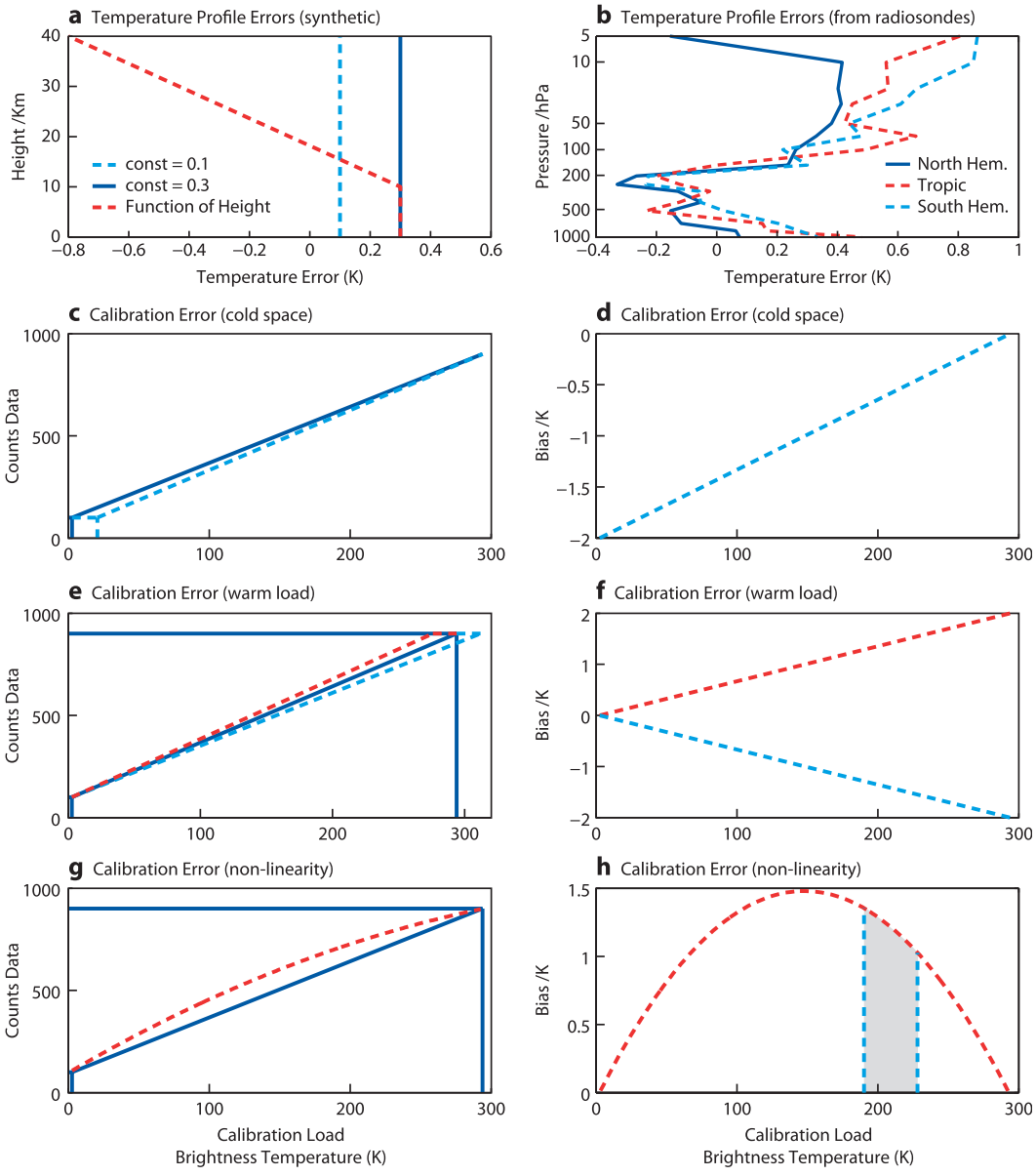

FIG. 6. The errors considered in the sensitivity study. (a), (b) Temperature errors introduced in the model profile, either synthetic or based on radiosonde mean departures, respectively. (c),(d) Errors expected to result from an error in the cold space measurement. (e),(f) Errors expected from a warm load calibration error, with the target temperature assumed erroneously cold and warm. (g),(h) Effect of radiometer nonlinearity, approximated by a quadratic function. The dynamic range of brightness temperatures MWTS channel 4 is indicated in the shaded area in (h). (c)–(h) True calibration curve (dashed lines) in contrast to the assumed curve (solid lines), which neglects specific errors.

magnitude of the errors studied is described in the subsections below.

a. Forecast model temperature errors

Errors in the temperature fields themselves will directly influence the fit of the model to observations. Several plausible forms of forecast model temperature error were tested. First, it could be assumed that differences between model temperatures and radiosonde measurements give an estimate of the true model error. The assumption here is that radiosonde measurements, taken over sufficiently large ensembles, have negligible systematic errors. Statistics on radiosonde fit to model temperatures are readily available and are shown in Fig. 6b. Tropospheric biases are generally below 0.5 K and are largest at the surface in both the Southern Hemisphere

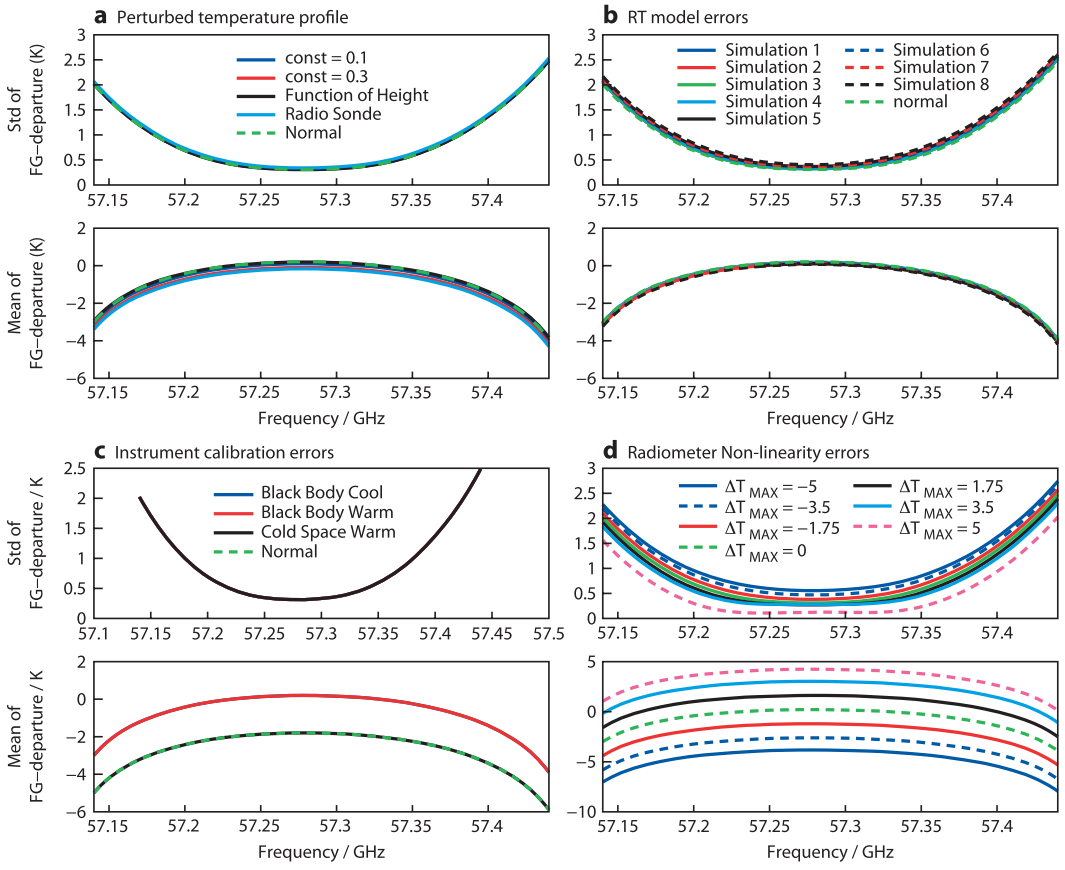

FIG. 7. The results of the sensitivity study showing how errors in (a) forecast model temperature profile, (b) radiative transfer model (based on simulations using the scaling factors given in Table 2), (c) instrument calibration, and (d) radiometer nonlinearity are manifested in the plot of (top) standard deviation and (bottom) mean of first-guess departures vs passband shift. (d) A $\Delta T_{\max}$ of 5 has been displaced down by 0.2 K to illustrate that a shallow double minimum for this channel appears for very large nonlinearities (magenta line).

and tropics. In the lower stratosphere the biases are generally <0.8 K, and significantly smaller in the Northern Hemisphere. As a second approach global errors of 0.1 and 0.3 K were assumed (see Fig. 6a). Finally, an error of 0.3 K in the troposphere, decreasing monotonically above 10 km to −0.8 K at 40 km, was assumed. The envelope of standard deviations of the resulting first-guess departures is shown in Fig. 7a. None of these hypothetical errors are able to project onto the double minimum feature in the plot of standard deviations of departures for MWTS-4 versus assumed passband shift. Of course, these hypothetical errors have very specific forms, and the results here do not conclusively prove the general point that model temperature errors cannot to be manifested as a passband shift–type error, but the point is demonstrated that simple model errors do not easily explain the form of the biases. The absence of similar patterns in the first-guess departure fields for AMSU-A is a stronger indication that model error is not the likely cause of the biases.

b. *Radiative transfer model errors*

In the MPM92 (Liebe 1989; Liebe et al. 1992) the emission along the observed atmospheric path is derived from the complex refractivity (N_D, ppm) for dry air, which is given by

$$N_D = N_d + \sum_k S_k F_k + N_n. \quad (1)$$

The second term on the right-hand side of Eq. (1) describes the resonant absorption from discrete rotational transition lines, each described by line strength (S_k) and line shape function (F_k); here, N_d is a nondispersive term and N_n is the O_2 nonresonant term. For observations in the 50–60-GHz part of the microwave spectrum the main contribution to N_D results from 44 discrete O_2 spectral lines. Respectively, S_k and F_k are given by

$$S_k = (a_1/\nu_k) p_d \theta^3 \exp[a_2(1 - \theta)], \quad (2)$$

TABLE 2. Scaling factors for the sensitivity study investigating errors in the line-by-line radiative transfer model (a_1 and a_3 scaling factors).

Parameter–simulation	1	2	3	4	5	6	7	8
a_1	1.00	1.00	1.02	1.02	1.02	1.05	1.05	1.05
a_3	1.02	1.05	1.00	1.02	1.05	1.00	1.02	1.05

$$F_k(\upsilon) = \upsilon\left(\frac{1 - i\delta_k}{\upsilon_k - \upsilon - i\gamma_k} - \frac{1 + i\delta_k}{\upsilon_k + \upsilon + i\gamma_k}\right), \quad (3)$$

where θ is a reciprocal temperature variable ($\theta = 300/T$) with temperature T in kelvins, and p_d is the partial pressure for dry air. The original Van-Vleck–Weisskopf line shape function (Van-Vleck and Weisskopf 1945), which is a function of frequency (υ), with parameters associated with the line center frequency (υ_k) and line width (γ_k), has been modified by Rosenkranz (1993) to include line overlap effects by additionally including the parameter δ_k. In MPM92 the line width (γ, GHz) and overlap (δ) parameters for pressure broadened O_2 lines in air are

$$\gamma_k = a_3 \times 10^{-3}(p_d\theta^{a_4} + e\theta), \quad (4)$$

$$\delta_k = (a_5 + a_6\theta)p\theta^{0.8}, \quad (5)$$

where e is the partial pressure of water vapor (mbar).

The parameters a_i are specified in MPM92 based on an analysis of laboratory spectra (Liebe et al. 1993). The uncertainties associated with the parameters a_i are discussed in Liebe et al. (1993), where it is suggested that the measurement uncertainties are ~2% for line strength and ~5% for line width. In this part of the study the most significant parameters (a_1 and a_3) governing the computation of absorption cross sections were perturbed by a maximum of 5%, as indicated in Table 2. The results shown in Fig. 7b demonstrate that errors of this type and magnitude do not project onto an apparent passband shift error. This is, at first sight, surprising because a line strength error would be expected to be manifested as an optical depth error similar to that caused by passband shift. The likely explanation is that much larger errors in the line parameters, not supported by the spectroscopic measurements reported in Liebe et al. (1993), would be required to cause the observed biases.

It is noteworthy that the absence of similar biases in the equivalent AMSU-A observations independently reduces the likelihood that the observed MWTS biases are related to model error or radiative transfer model error because these errors are common to both MWTS and AMSU-A.

c. Instrument calibration errors

Several types of instrument error related to the radiometric calibration of the instrument can be envisaged. These are illustrated schematically in Fig. 6. Figures 6c,d illustrate the consequences of a calibration error affecting the cold space calibration point, for example, through field-of-view contamination by some part of the spacecraft. The result of such effects is that for a given scene count, the derived scene temperature would be converted to an erroneously low brightness temperature and the magnitude of the error would increase monotonically because observed temperatures tended toward the temperature of cold space. Of course, for the channels studied here, the range of observed brightness temperatures have a lower limit of 160 K.

Figures 6e,f illustrate schematically the consequences of a warm load calibration error. This type of error could result from thermal gradients across the warm calibration load causing a load radiometric temperature warmer (or colder) than the temperature measured by the platinum resistance thermometers embedded in the calibration load. The resulting biases increase monotonically from cold space as scene temperatures increase. The results, shown in Fig. 7c, demonstrate that this class of calibration error cannot account for the double minimum structure in MWTS-4.

Figures 6g,h show the effect of detector nonlinearity. The detector response $[\partial(\text{counts})/\partial(T_{sc})]$ is larger at low measured scene temperatures (T_{sc}). At the calibration load temperatures (2.7 and 300 K) the error is close to zero, but a maximum is shown at the midpoint (~148 K). For a channel such as MWTS channel 4, where the range of scene temperatures is 185–240 K, this type of error would be manifested as (i) a positive bias and (ii) an increase in the bias toward lower temperatures. A negative bias could be envisaged, but is less likely because it would require the radiometer sensitivity to *increase* with increasing scene radiance rather than the saturation effect normally observed. This bias is quadratic in form, but over a narrow dynamic range it could be manifested as an approximately linear variation in the error versus scene temperature. The results are shown in Fig. 7d. For large nonlinearities (ΔT_{max} = 5 K) the standard deviation curves begin to show a double minimum structure, similar to that for MWTS-4. Although such large nonlinearities are unlikely to be the cause of the apparent passband shift, the results of the sensitivity study drew our attention to the possibility of radiometer nonlinearity contributing to the observed biases.

d. Nonlinearity errors

The passband shifts derived above (section 2, Fig. 4) were applied to the simulations for MWTS channels 2–4. The residual first-guess departures are shown in

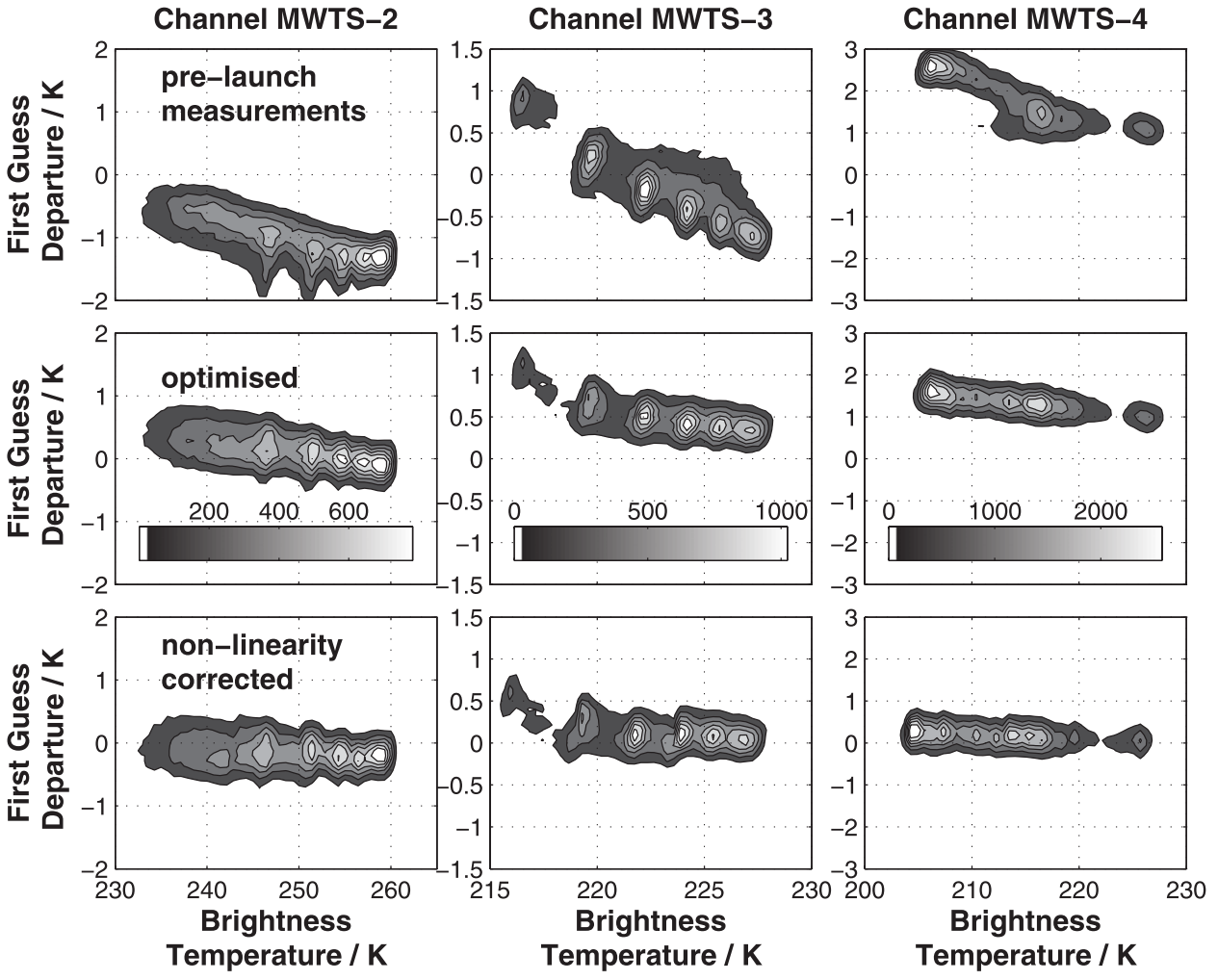

FIG. 8. 2D histograms of first-guess departures vs scene brightness temperature for (from left to right) MWTS channels 2, 3, and 4 for prelaunch measured (top) passbands, (middle) optimized passbands, and (bottom) nonlinearity corrected data. The contours are generated from a 50×50 grid over the range of brightness temperatures and first-guess departures shown. The number of observations per bin is indicated in color bars in the middle plots.

Fig. 8 plotted against measured scene temperature. Prior to the application of an optimized estimate of the passband center frequencies, the first-guess departures show a complex dependency on the scene temperature, consistent with the passband shift error being directly dependent on vertical temperature gradients rather than temperature directly. After applying the more optimal passband parameters, the data collapses onto a clear *near-linear* relationship, consistent with the expected local appearance of a quadratic error term resulting from radiometer nonlinearity. Removal of a quadratic error term of magnitude ($\Delta T_{\max}$) in the range from -0.3 to 1.5 K results in unbiased data with a much-reduced dependency on measured scene temperature, as will be demonstrated in the next section.

4. Optimization

Following the results described above in section 3d a simple scheme was devised to simultaneously estimate the parameters describing the passband shift ($\Delta\upsilon_0$) and the nonlinearity error ($\Delta T_{\max}$, described in the appendix). The scheme involved computing the mean and standard deviation of observations minus simulations from an ensemble of 15 000 observations. Simulations were carried out using the MPM92 LBL model. Bandwidths for each channel were taken from specified values, and this parameter was not varied in the optimization. Nonlinearity errors were computed using a quadratic error (see the appendix). This quadratic form was derived assuming that errors are zero at calibration points (at temperatures of 2.7 and 294 K for the cold

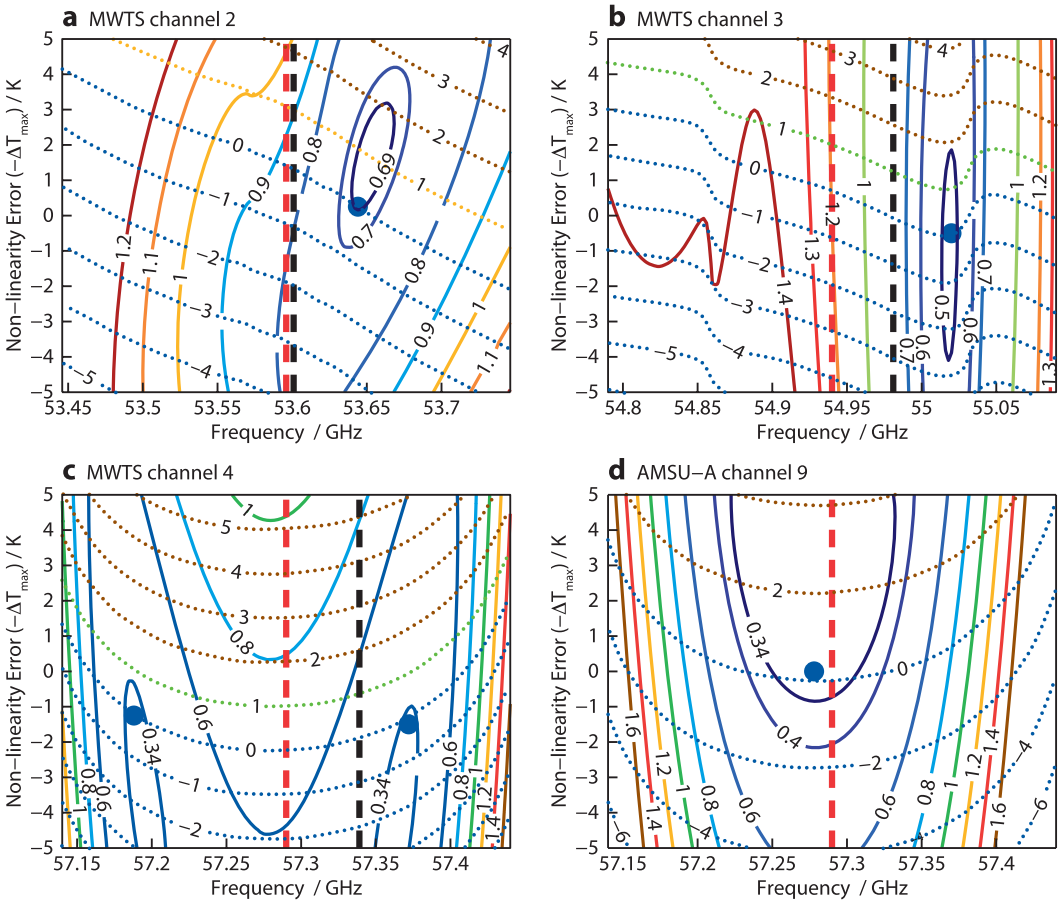

FIG. 9. Results of the optimization for (a)–(c) MWTS channels 2–4, respectively, and (d) AMSU-A channel 9. Each plot shows the standard deviation (solid colored contours) and mean (dotted colored contours) of departures against the passband center frequency (x axis) and nonlinearity parameter ($\Delta T_{\max}$, y axis). The position of the design-specified passband center is shown (red vertical dotted line); the prelaunch measurements are shown (black dotted line). The optimized estimates of the passband center and nonlinearity parameter for each channel (dots).

space and warm load views, respectively), and is characterized by a single parameter ($\Delta T_{\max}$), which is the maximum brightness temperature error, expected at $T_{sc} = 0.5(T_{cold} + T_{warm})$. The computed mean [$m(\Delta\upsilon_0, \Delta T_{\max})$] and standard deviation [$s(\Delta\upsilon_0, \Delta T_{\max})$] of the departures are shown in Fig. 9. Because both factors are important in constraining the optimal estimate of the instrument parameters these were combined in an empirical penalty function $J(\Delta\upsilon_0, \Delta T_{\max})$, as

$$J(\Delta\upsilon_0, \Delta T_{\max}) = \frac{m(\Delta\upsilon_0, \Delta T_{\max})^2}{\sigma_m^2} + \frac{s(\Delta\upsilon_0, \Delta T_{\max})^2}{\sigma_s^2}, \quad (6)$$

where σ_m and σ_s are chosen to represent our estimate, based on an educated guess, of the uncertainties in the expected residual bias and tolerable increase in standard deviation relative to the absolute minimum obtained over the parameter space. These values were chosen to be 0.25 K for the uncertainty in the residual bias and 2% of the minimum standard deviation over the parameter space. A tolerable residual bias (before variational bias correction) of 0.25 K is in broad agreement with the bias corrections currently applied to other similar radiance observation types in the ECMWF system (e.g., AMSU-A, AIRS, and IASI). In addition the uncertainties in the brightness temperatures of the blackbody targets used for the instrument end-to-end calibration is around 0.3 K at 95% confidence. Calculations were performed to estimate the variation in the derived instrument parameters for variations in σ_m and σ_s. This showed the estimates to be relatively robust for large changes ($\times 5$) in either parameter. This results from the relatively deep (shallow) minimum in the standard deviations with respect to passband shift (nonlinearity). On the other hand, the mean difference shows relatively slow (fast)

TABLE 3. Modified MWTS channel characteristics.

	MWTS channel		
	2	3	4
Design passband (GHz)	53.596	54.94	57.29
Prelaunch measurement (GHz)	53.601	54.981	57.340
Optimized estimate (GHz)	53.656	55.020	57.373
Rescaled (GHz)	53.633	55.013	57.373
Nonlinearity (ΔT_{max}; K)	−0.3	0.6	1.5

variations with respect to passband shift (nonlinearity). The mean and standard deviations of the observed − simulated differences give the following two independent pieces of information to help estimate the new parameters: the standard deviation yields information about how the new parameters fit the *structure* of the departure fields, whereas the mean gives information about how well the new parameters allow the simulations to fit the overall magnitude of the observed brightness temperature field.

The code was parallelized to run on the ECMWF IBM high-performance supercomputer. Simulations took ~10 h for an ensemble of 15 000 observations for MWTS channels 2–4. Figure 9 shows contours of mean and standard deviation of the departures versus passband shift and nonlinearity parameters. The points indicate the position of the minimum in the penalty function defined in Eq. (6). The associated values for the new passband and nonlinearity parameters are given in Table 3.

In deciding on an optimized set of instrument parameters interchannel consistency was also a consideration. For channel 4 the double minimum in Fig. 9c supports two possible choices of $\Delta\upsilon_0$ and ΔT_{max}, one associated with negative passband shifts and the other positive. The shifts for channels 2 and 3 are both positive, at +45 and +51 MHz, respectively, and this suggests the shift for channel 4 is also likely to be positive. Conceivable physical mechanisms that could explain the shift, for example, calibration errors in the prelaunch measurement of the local oscillators (LOs) or on-orbit temperature tuning of the LOs, are most likely to affect all channels similarly.

Note in Table 3 that the passbands for channels 2, 3, and 4 are shifted by +55, +39, and +33 MHz relative to prelaunch measurements, and by +60, +80, and +83 MHz relative to design specification, respectively. The nonlinearities (expressed as ΔT_{max}) are −0.3, 0.6, and 1.5 K, respectively.

The uncertainties in the optimized parameters were estimated through an analysis of the reproducibility of the optimization. Over 28 independent consecutive 12-h cycles during February 2010 the standard deviation of the passband shift was 4.6, 0.66, and 1.57 MHz for channels 2, 3, and 4, respectively. The larger scatter in the optimized parameters for channel 2 results from the contamination of the measured radiances by clouds. The optimized parameters derived from February 2010 were checked using data from a cycle on 17 September 2008 and were found to be stable. In the absence of significant systematic error in these estimates, these reproducibility values would translate to uncertainty estimates below 1 MHz for channels 2–4 (by taking the standard error of the mean of the estimates); however, the uncertainty is most likely dominated by systematic components. A significant systematic error is associated with the choice of tolerable residual bias. If a tolerable residual bias of 0.25 K is assumed, then the resulting uncertainty in the estimates of $\Delta\upsilon_0$ and ΔT_{max} can be obtained by projecting this bias, taken along the semimajor axis of the minima of Fig. 9 onto the y and x axes of Fig. 9, respectively. The resulting uncertainty estimates, at 95%, are 2.5 MHz in passband shift and 0.5 K in ΔT_{max}; however, it should be emphasized that this is a crude estimate and further work is needed to understand all possible systematic contributions to the error in this estimate.

In the later stages of this study, the instrument manufacturer revealed that a likely explanation for the apparent passband shift on orbit was linked to the resonant cavity used to tune the frequency of the local oscillator. The frequency of the oscillator is governed by the modes of the cavity, which are dependent upon the cavity length and refractive index. The change in the refractive index of the medium filling the cavity (air for the laboratory-based prelaunch measurements and near-vacuum conditions on orbit) was used to compute new passband center frequencies, which are shown in Table 3 (see the rescaled estimates of the passband center). These shifts are +32, +32, and +33 MHz for channels 2–4, respectively. These values are in excellent agreement with the optimized estimate provided here for channel 4, less good for channel 3, and well outside our initial estimated error bounds for channel 2. The reason for the poor agreement for channel 2 could be related to an optimistic estimate of the tolerable residual bias and the higher sensitivity of the channel 2 estimate to this assumption, but further work is needed to confirm this. Nevertheless, the study presented here based on NWP fields and radiative transfer modeling has clearly highlighted a problem with the initial specifications.

5. Results and discussion

The overall effect of the revised instrument parameters is illustrated in Figs. 10a–c, which shows the MWTS channels 2–4 first-guess departures for passband center frequencies given by design specification, prelaunch

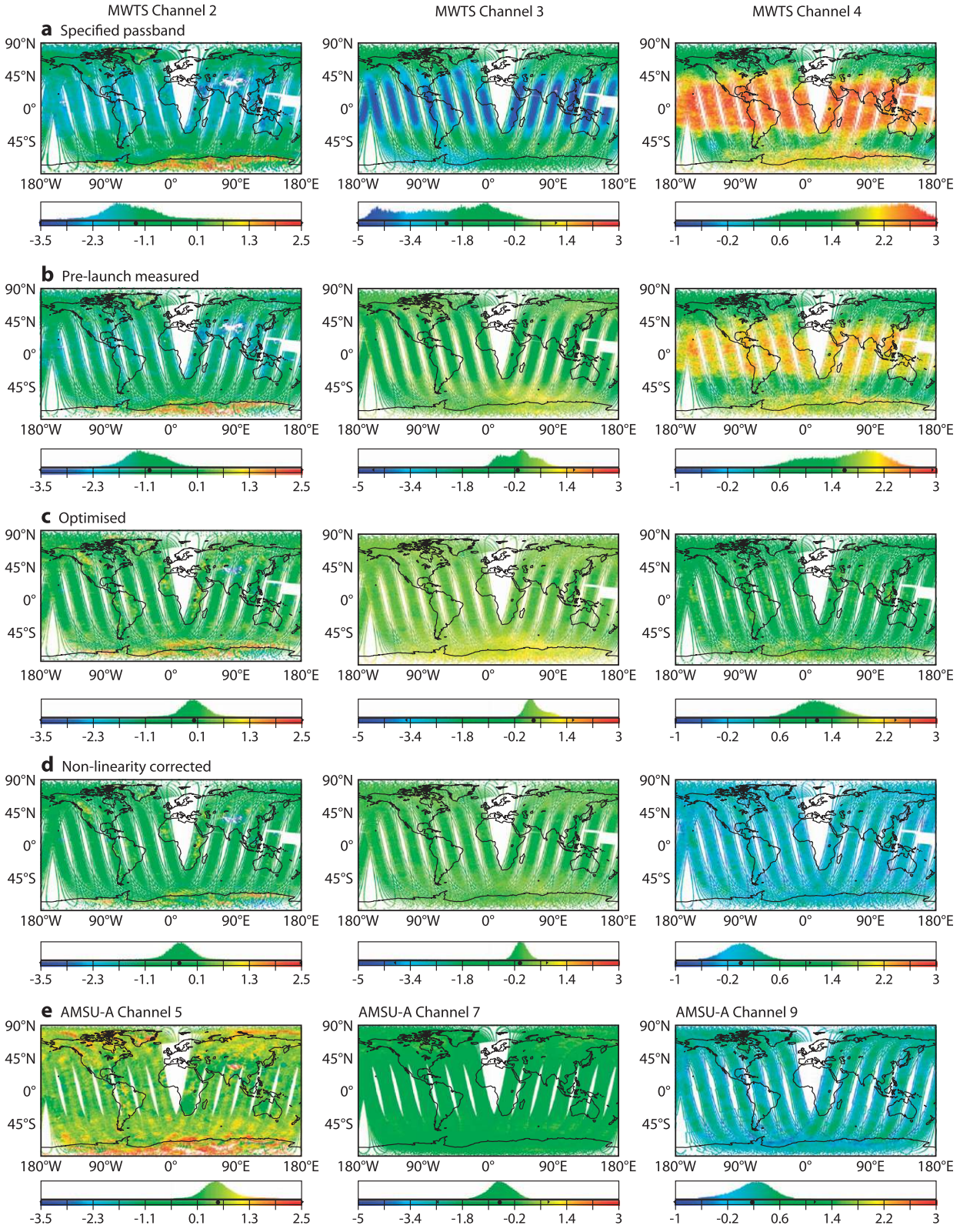

FIG. 10. Maps of first-guess departures (K) for (from left to right) MWTS channels 2–4 showing departures using (a) design-specified passbands, (b) the prelaunch-measured passbands, (c) the optimized passbands, (d) passbands following nonlinearity correction, and (e) the equivalent *MetOp-A* first-guess departure maps. The spots at the base of the histograms indicate the mean first-guess departure.

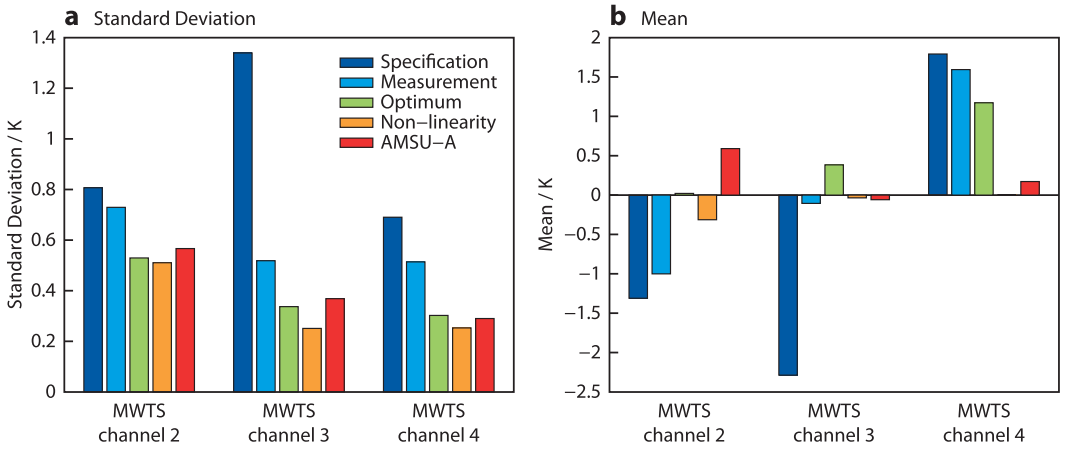

FIG. 11. (a) Standard deviations and (b) means of first-guess departures for MWTS channels 2, 3, and 4 for design-specified passbands, prelaunch-measured passbands, optimized passbands, and nonlinearity corrected passbands. Also shown are the statistics for equivalent *MetOp-A* AMSU-A channels.

measurements, and optimized estimates. Figure 10d shows the departures after nonlinearity correction (prior to variational bias correction) and, for comparison, the equivalent AMSU-A first-guess departures are shown (Fig. 10e). Figure 10 shows the significant and continuous improvement in first-guess departures from simulations using the specified passbands, through the use of prelaunch measurements to optimized estimates of the passband centers, and finally the inclusion of an optimized nonlinearity correction. The statistics (mean and standard deviation) are summarized in Fig. 11. The standard deviations for MWTS channels 2, 3, and 4 are reduced by 37%, 81%, and 64% relative to design specifications and by 30%, 52%, and 51% relative to prelaunch measurements. Standard deviations for the corrected data are 0.51, 0.25, and 0.25 K, which compare favorably with the equivalent AMSU-A values of 0.56, 0.36, and 0.29 K. Mean biases are reduced to −0.31, −0.035, and 0.003 K, which again compare favorably to AMSU-A equivalents of 0.59, −0.059, and 0.172 K. The systematic biases corrected here were found to be stable, and the applied corrections resulted in similar improvements to first-guess departures for data obtained 18 months apart.

It is expected that the use of variational bias correction will further reduce the spread in both MWTS and AMSU-A departures because of residual forecast and RT model biases as well as instrument effects. Further reductions of ~30% in the standard deviations for AMSU-A channels 5, 7, and 9 are expected, based on previous experience. The on-orbit noise performance of the MWTS radiometer was estimated by computing histograms of standard deviations of the observed brightness temperature for small ensembles of observations, as described in Bell et al. (2008) (see Fig. 12). Also shown for comparison in Fig. 12 is an analysis of equivalent channels from *NOAA-19* AMSU-A. The MWTS on-orbit NEΔT values (in the range of 0.14–0.19 K) are significantly lower than the design specification of 0.4 K. These NEΔT values represent the lower limit to the achievable standard deviations for the first-guess departures. The estimates for *NOAA-19* channels 5, 7, and 9 were cross checked with values derived from on-orbit data over the same period, using the method described in Atkinson and McLellan (1998). The agreement was better than 0.045 K for these channels.

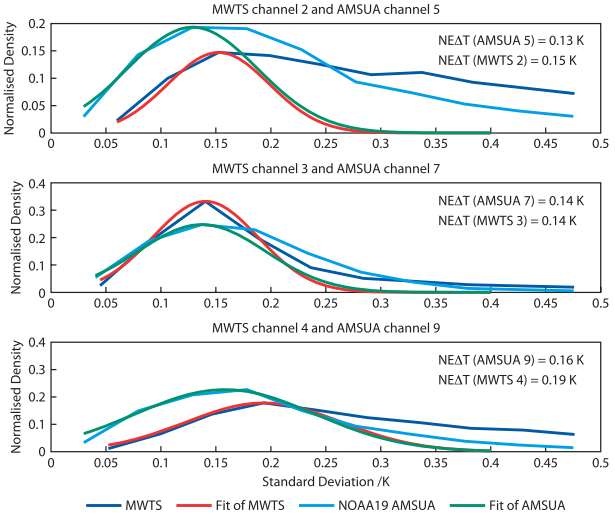

FIG. 12. Estimates of NEΔT for MWTS channels 2–4 and *NOAA-19* AMSU-A channels 5, 7, and 9. Each plot shows the standard deviation for ensembles of clusters (of six fields of view) of MWTS/AMSU-A observations. The low standard deviation edge of the curves are fitted to a Gaussian function to estimate the NEΔT (indicated).

For operational purposes the passband shift is best dealt with through an update to the regression coefficients used in fast radiative transfer models. The nonlinearity correction is best handled within the ground processing systems, ideally based on accurate prelaunch radiometric measurements. In the short term, tests at ECMWF have commenced using the brightness temperature corrections derived here.

Further numerical experiments are required to assess how much further the MWTS standard deviations are reduced prior to assimilation. The effect of the revised passband frequencies on the weighting functions for MWTS channels 2–4 is shown in Fig. 2. The new passband specifications result in an upward displacement of the weighting functions.

In summary the quality of the level 1B MWTS data has been significantly improved by two physically based corrections to the data: passband shift and radiometer nonlinearity. The novel approach presented here illustrates the usefulness of NWP model fields and radiative transfer modeling in characterizing the satellite sounders on orbit. The methodology has been demonstrated for *FY-3A* MWTS but is applicable to other microwave temperature sounders, for example, subsequent *FY-3* sensors, AMSU-A, the Special Sensor Microwave Imager/Sounder (SSM/IS), and the Advanced Technology Microwave Sounder (ATMS). The method could be adapted to *operationally* monitor the orbital and long-term stability of these instrument parameters.

NWP models should continue to play a role in the calibration and validation of satellite sounding instruments, complementing other established techniques for characterizing instrument performance. One advantage offered by this type of analysis is that the global nature of the analysis means that most of the dynamic range of measured brightness temperatures and atmospheric variability is probed in each analysis cycle, enabling passband errors and nonlinearity errors to be characterized very efficiently.

This study also illustrates the increasing requirement for improved prelaunch calibration of satellite instruments for operational meteorology. It could be argued, based on these results, that this technique alleviates the need for accurate prelaunch measurements; however, the widespread application of this type of data for climate research and reanalysis means the data will, in time, be subject to intense scrutiny. This being the case, it is best that this type of analysis is used in conjunction with careful prelaunch characterization [Saunders et al. (1995) and Mo (1996) provide examples of best practice] ideally based on metrologically traceable measurements of the instrument and relevant subsystems.

Regarding further work, the extension of this technique to other sensors as well as establishing operational monitoring capabilities have been mentioned above. Uncertainties in the estimate of the passband shift and nonlinearity parameters have been discussed, but more work could be done to determine more robust uncertainties. Finally, additional work will be carried out to quantify the impact of the revised data on NWP analysis and forecast quality.

Acknowledgments. This study was made possible by support from the EUMETSAT NWP Satellite Application Facility (NWPSAF) visiting scientist program for Qifeng Lu's visit to ECMWF. The authors thank Tony McNally of ECMWF for arranging this visit. This work was also supported by the bilateral cooperation agreement between ECMWF and the China Meteorological Administration (CMA) and by the National Natural Science Foundation of China (Grant 40705037). The work was also supported by China's Research and Development Special Fund for Public Welfare Industry [Meteorology GYHY(QX)2007-6-9 and GYHY200906006]. Nigel Atkinson at the Met Office kindly provided estimates of *NOAA-19* AMSU-A radiometric noise.

APPENDIX

Parameterization of Nonlinearity Errors

This appendix shows that the nonlinearity error can be characterized by a single parameter $\Delta T_{\max}$, which defines the coefficients in a quadratic approximation for the error.

It is assumed here that the radiometer nonlinearity error (ΔT) is well approximated by a quadratic expression in the measured scene temperature (T),

$$\Delta T = c_0 + c_1 T + c_2 T^2. \tag{A1}$$

This error is subject to the constraint that the error is zero at the cold space (T_c) and warm load (T_w) temperatures,

$$c_0 + c_1 T_c + c_2 T_c^2 = 0. \tag{A2}$$

$$c_0 + c_1 T_w + c_2 T_w^2 = 0. \tag{A3}$$

The error can then be defined in terms of a single parameter $\Delta T_{\max}$, which represents the maximum amplitude of the error over the range $[T_c, T_w]$. This value for the maximum error, found at $T = (T_c + T_w)/2$, introduces a third equation:

$$c_0 + c_1\left(\frac{T_c + T_w}{2}\right) + c_2\left(\frac{T_c + T_w}{2}\right)^2 = \Delta T_{\max}. \quad \text{(A4)}$$

Equations (A2), (A3), and (A4) can be solved for the coefficients c_0, c_1, and c_2 to give

$$c_0 = \frac{-4\Delta T_{\max} T_c T_w}{(T_c - T_w)(T_c + T_w)}, \quad \text{(A5)}$$

$$c_1 = \frac{\Delta T_{\max}}{T_c - T_w}, \quad \text{(A6)}$$

$$c_2 = \frac{-4\Delta T_{\max}}{(T_c - T_w)(T_c + T_w)}. \quad \text{(A7)}$$

This formulation of the nonlinearity error was used in the optimization described in section 4 and summarized in Fig. 9 in order to reduce the degrees of freedom for the optimization using the strong constraint that the error (ΔT) is identically zero at T_c and T_w. For the nonlinearity corrections illustrated in Fig. 8 the coefficients c_0, c_1, and c_2 in Eq. (A1) were allowed to vary independently using a weaker constraint on the value of ΔT at T_c and T_w. This allows the fit to account for radiometric offsets and errors linear in the scene brightness temperature known to affect microwave radiometers. The numerical values for c_0, c_1, and c_2 are given in Table A1.

This scheme outlined in Eqs. (A1)–(A7) is similar, in some respects, to that presented in Zou et al. (2009) for the recalibration of MSU data in which (following the notation of Zou et al. 2009) the earth scene radiance (R) is given by

$$R = R_L - \delta R + \mu Z, \quad \text{(A8)}$$

where R_L is the dominant linear response

$$R_L = R_c + S(C_e - C_c). \quad \text{(A9)}$$

The nonlinear response is given by

$$Z = S^2(C_e - C_c) - (C_e - C_w), \quad \text{(A10)}$$

where

$$S = \frac{(R_w - R_c)}{(C_w - C_c)}, \quad \text{(A11)}$$

and C_e, C_c, and C_w are the counts corresponding to the earth scene, cold space, and warm calibration targets, respectively; R_c and R_w are the radiances associated with the cold space views and warm target views, respectively; and δR represents a radiance offset. The nonlinear coefficient μ was found to be a function of the MSU instrument temperature. This scheme and that presented in Eqs. (A1)–(A7) share the property that the nonlinearity error is zero at the calibration points.

TABLE A1. Coefficients used in the nonlinearity corrections.

	MWTS channel		
	2	3	4
a_0	0.079 546 796	0.070 824 104	0.000 859 831
a_1	0.015 843 045	0.025 371 222	0.027 636 840
a_2	−0.000 060 438 557	−0.000 107 616 679	−0.000 103 839 638

REFERENCES

Atkinson, N., and S. McLellan, 1998: Initial evaluation of AMSU-B in-orbit data. *Microwave Remote Sensing of the Atmosphere and Environment,* T. Hayasaka et al., Eds., International Society for Optical Engineering (SPIE Proceedings, Vol. 3503), 276, doi:10.1117/12.319506.

Auligné, T., A. P. McNally, and D. P. Dee, 2007: Adaptive bias correction for satellite data in a numerical weather prediction system. *Quart. J. Roy. Meteor. Soc.,* **133,** 631–642.

Bell, W., and Coauthors, 2008: The assimilation of SSMIS radiances in numerical weather prediction models. *IEEE Trans. Geosci. Remote Sens.,* **46,** 884–900.

Cardinali, C., 2009: Monitoring the observation impact on the short-range forecasts. *Quart. J. Roy. Meteor. Soc.,* **135,** 239–250.

Collard, A. D., and A. P. McNally, 2009: The assimilation of Infrared Atmospheric Sounding Interferometer radiances at ECMWF. *Quart. J. Roy. Meteor. Soc.,* **135,** 1044–1058.

Dee, D. P., 2005: Bias and data assimilation. *Quart. J. Roy. Meteor. Soc.,* **131,** 3323–3343.

Dong, C., and Coauthors, 2009: An overview of Chinese new weather satellite *FY-3A*. *Bull. Amer. Meteor. Soc.,* **90,** 1531–1544.

English, S. J., R. Saunders, B. Candy, M. Forsythe, and A. Collard, 2004: Met Office satellite data observing system experiments. *Proc. Third WMO Workshop on the Impact of Various Observing Systems in Numerical Weather Prediction,* Alpbach, Austria, WMO, 146–156.

Geer, A. J., P. Bauer, and N. Bormann, 2010: Solar biases in microwave imager observations assimilated at ECMWF. *IEEE Trans. Geosci. Remote Sens.,* **48,** 2660–2669.

Goodrum, G., K. B. Kidwell, and W. Winston, 2000: NOAA KLM users guide. NOAA, section 3.3. [Available online at http://www.ncdc.noaa.gov/oa/pod-guide/ncdc/docs/klm/html/c3/sec3-3.htm.]

Grody, N. C., K. Y. Vinnikov, M. D. Goldberg, J. T. Sullivan, and J. D. Tarpley, 2004: Calibration of multisatellite observations for climatic studies: Microwave Sounding Unit (MSU). *J. Geophys. Res.,* **109,** D24104, doi:10.1029/2004JD005079.

Healy, S., and J.-N. Thépaut, 2006: Assimilation experiments with CHAMP GPS radio occultation measurements. *Quart. J. Roy. Meteor. Soc.,* **132,** 605–623.

Karl, T. R., S. J. Hassol, C. D. Miller, and W. L. Murray, 2006: Temperature trends in the lower atmosphere: Steps for understanding and reconciling differences. U.S. Climate Change Science Program: Synthesis and Assessment Product 1.1, 180 pp. [Available online at http://www.climatescience.gov/Library/sap/sap1-1/finalreport/default.htm.]

Liebe, H. J., 1989: MPM—An atmospheric millimeter-wave propagation model. *Int. J. Infrared Millimeter Waves,* **10,** 631–650.

——, P. W. Rosenkranz, and G. Hufford, 1992: Atmospheric 60-GHz oxygen spectrum: New laboratory measurements and line parameters. *J. Quant. Spectrosc. Radiat. Transfer,* **48,** 629–643.

——, G. Hufford, and M. Cotton, 1993: Propagation modeling of moist air and suspended water/ice particles at frequencies below 1000 GHz. *AGARD 52nd Specialists' Meeting of the Electromagnetic Wave Propagation Panel Symp.,* Palma de Mallorca, Spain, AGARD, Article 542. [Available online at http://www.its.bldrdoc.gov/pub/conference_papers/AGARD-542_liebe_hufford_cotton_1993/Liebe1993Agard.pdf.]

Mo, T., 1996: Prelaunch calibration of the Advanced Microwave Sounding Unit-A for NOAA-K. *IEEE Trans. Microwave Theory Tech.,* **44,** 1460–1469.

——, M. D. Goldberg, D. S. Crosby, and Z. Cheng, 2001: Recalibration of the NOAA Microwave Sounding Unit. *J. Geophys. Res.,* **106,** 10 145–10 150.

Peubey, C., W. Bell, P. Bauer, and S. Di Michele, 2011: A study on the spectral and radiometric specifications of a post-EPS microwave imaging mission. ECMWF Tech. Memo. 643.

Rosenkranz, P. W., 1993: Absorption of microwaves by atmospheric gases. *Atmospheric Remote Sensing by Microwave Radiometry,* M. A. Janssen, Ed., Wiley and Sons, 37–90.

Saunders, R., T. Hewison, S. Stringer, and N. Atkinson, 1995: The radiometric characterization of AMSU-B. *IEEE Trans. Microwave Theory Tech.,* **43,** 760–771.

Van-Vleck, J. H., and V. F. Weisskopf, 1945: On the shape of collision broadened lines. *Rev. Mod. Phys.,* **17** (2/3), 227–236.

Zou, C.-Z., M. D. Goldberg, Z. Cheng, N. C. Grody, J. T. Sullivan, C. Cao, and D. Tarpley, 2006: Recalibration of Microwave Sounding Unit for climate studies using simultaneous nadir overpasses. *J. Geophys. Res.,* **111,** D19114, doi:10.1029/2005JD006798.

——, M. Gao, and M. D. Goldberg, 2009: Error structure and atmospheric temperature trends in observations from the Microwave Sounding Unit. *J. Climate,* **22,** 1661–1681.